Journal of Alloys and Compounds 488 (2009) 619–623

Contents lists available at ScienceDirect

Journal of Alloys and Compounds

journal homepage: www.elsevier.com/locate/jallcom

Structural and optical properties of $GdAlO_3:RE^{3+}$ (RE = Eu or Tb) prepared by the Pechini method for application as X-ray phosphors

H.H.S. Oliveira, M.A. Cebim, A.A. Da Silva, M.R. Davolos*

Unesp - São Paulo State University, Instituto de Química, 14800-900, Araraquara, São Paulo, Brazil

ARTICLE INFO

Article history:
Received 5 June 2008
Received in revised form 17 April 2009
Accepted 17 April 2009
Available online 24 April 2009

Keywords:
Rare earth alloys and compounds
Chemical synthesis
Optical properties
Luminescence
Optical spectroscopy

ABSTRACT

In this work, $GdAlO_3:RE^{3+}$ (RE = Eu or Tb) was successfully prepared by the Pechini method at lower temperatures when compared to others methods as solid-state synthesis and sol–gel process. In accordance to the XRD data, the fully crystalline single-phase $GdAlO_3$ could be obtained at 900 °C. The differential thermal analysis (DTA) shows a crystallization peak at 850 °C. The samples are composed by monocrystalline particles (50–120 nm) exhibiting the formation of aggregates among them, which indicates the beginning of the sinterization process. This feature indicates a strong tendency to the formation of aggregates, which is a suitable ability for the close-packing of particles, and hence a potential application in X-ray intensifying screens. Luminescence measurements indicate $Gd^{3+} \rightarrow RE^{3+}$ energy transfer. The Eu^{3+} emission spectra exhibit all the characteristics $^5D_0 \rightarrow {}^7F_j$ transitions and the observed profile suggests that RE^{3+} ions occupy at least one site without center of symmetry. For terbium-doped samples, the $^5D_3 \rightarrow {}^7F_j$ (blue emission) and $^5D_4 \rightarrow {}^7F_j$ (green emission) transitions were observed and the ratio between them may depend on the Tb^{3+} content due to cross-relaxation processes.

1. Introduction

X-ray phosphors are compounds that can efficiently convert high-energy photons (X-ray photons) in UV–visible radiations. This property allows such materials to be applied in industrial inspection, dosimetry, high-energy physics, nuclear medicine and medical diagnostics [1]. All medical imaging modalities that require the detection of energetic photons use these materials for their detection [2,3].

Each application requests a material with certain optical and structural properties. In general, no phosphor fulfills the requirements for all applications. Thus, improvements in one or more properties are desirable in the quest for efficient X-ray phosphors [4], which must have properties that include high density, chemical stability, radiation hardness, high luminescent yield and in some cases short lifetime. Besides, they must be easily obtained and have low cost [5,6].

Perovskite rare-earth aluminates are compounds endowed with high density and chemical stability, being promising hosts for X-ray phosphors [7,8]. These aluminates present general formula $REAlO_3$ (where RE represent rare-earth ions), where each RE ion is surrounded by 12 O^{2-} anions and each Al^{3+} ion by 6 O^{2-} anions (AlO_6 octahedral group). The structures of most $REAlO_3$ compounds, named orthorhombic perovskites, belong to the space group *Pbnm* due to distortions in the AlO_6 octahedra, and are derived from the ideal cubic perovskites (*Pm3m*).

Among these inorganic materials, the rare earth doped gadolinium aluminates, $GdAlO_3:RE^{3+}$ (RE = Eu or Tb), are promising for application as X-ray phosphors because it presents high density, chemical stability and important electronic and spectroscopic properties [9] as color purity, high luminous yield, lifetime of ms and $Gd^{3+} \rightarrow RE^{3+}$ energy transfer.

The Eu^{3+} ions exhibit intense red emission with lifetime of milliseconds. Moreover, Eu^{3+} ions are used as spectroscopy probe in the structural characterization of materials. The Tb^{3+} ions exhibit intense green or blue emission and they also present lifetime of milliseconds and high quantum yield values. Actually, the material utilized in planar X-ray imaging is doped with Tb^{3+} ions, $Gd_2O_2S:Tb^{3+}$.

The $REAlO_3:RE^{3+}$ has been obtained by solid-state synthesis in elevated temperatures (above 1400 °C). Wet chemical routes can be more advantageous because they make possible the preparations of phases in low temperatures and with effective doping. For example, the fully crystalline single-phase $GdAlO_3$ was obtained at 900–1000 °C via sol–gel method by Cizauskaite et al. [7]. Hai et al. obtained $Lu_2O_3:Eu^{3+}$ films by Pechini method and observed crystalline phase starting from 400 °C [10]. In this way, we propose a systematic study of the evolution of structural and optical properties of Eu^{3+}- and Tb^{3+}-doped $GdAlO_3$ powders prepared by the Pechini method with the firing temperature.

* Corresponding author. Tel.: +55 1633016634; fax: +55 1633227932.
E-mail address: davolos@iq.unesp.br (M.R. Davolos).

0925-8388/$ – see front matter © 2009 Elsevier B.V. All rights reserved.
doi:10.1016/j.jallcom.2009.04.099

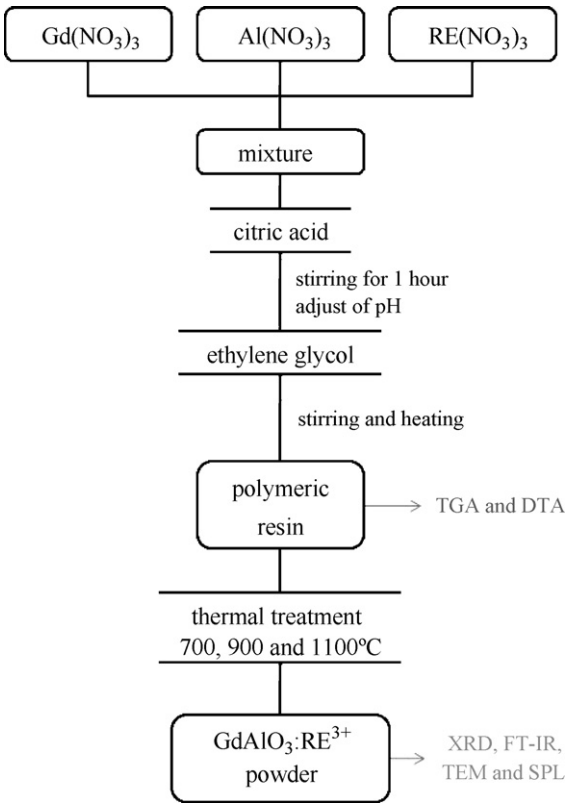

Fig. 1. Flow scheme of synthesis procedure of $GdAlO_3:RE^{3+}$.

2. Experimental

Rare-earth oxides (Aldrich 99.999%) and aluminum nitrate (Merk 99.5%) were used as start materials. Other chemicals used were grade reagents. Approximately 0.3 g of $GdAlO_3:RE^{3+}$ (where RE = Eu or Tb) samples were prepared using a wet chemical route, i.e., the Pechini method [10,11], with 1.0, 3.0 and 5.0 at% dopant concentration. Solutions of $Gd(NO_3)_3$, $Al(NO_3)_3$ and $RE(NO_3)_3$ were mixed in stoichiometric amounts with citric acid (CA) and ethylene glycol (EG), obeying the molar proportion 1:3:16 metal:CA:EG. Initially, citric acid was added to the aqueous solution of Gd^{3+}, Al^{3+} and TR^{3+} metals. The pH was adjusted for 5.5 with NH_4OH 0.1 mol L^{-1} and the mixture was stirred for 1 h. Afterwards, ethylene glycol was added and the solution stayed under continuous stirring and heating (~100 °C) for solvent evaporation. The obtained polymeric resin was fired in air atmosphere at 700, 900 and 1100 °C in a tubular oven for 4 h. Fig. 1 shows the flow scheme for the process of preparing $GdAlO_3:RE^{3+}$. Thermogravimetric and differential thermal analysis of polymeric resins were carried out using a SDT 2960 simultaneous TGA–DTA in the temperature range 25–1180 °C at a heating rate of 10 °C min^{-1} under an air flux. The powders samples were characterized by X-ray diffractometry (XRD) using Cu Kα radiation (λ = 1.5442 Å) in a Siemens D5000 diffractometer. Infrared spectra (FT-IR) were obtained using a spectrophotometer Perkin Elmer FT-IR Spectrum 2000. The samples also were characterized by transmission electronic microscopy (TEM) and energy dispersive X-ray spectroscopy (EDS) using a Philips CM 200 microscope. The photoluminescence measurements (PL) were recorded in a Fluorog SPEX F212I fluorescence spectrophotometer equipped with R928 Hamamatsu photomultiplier. The excitation and emission spectra were measured at room temperature.

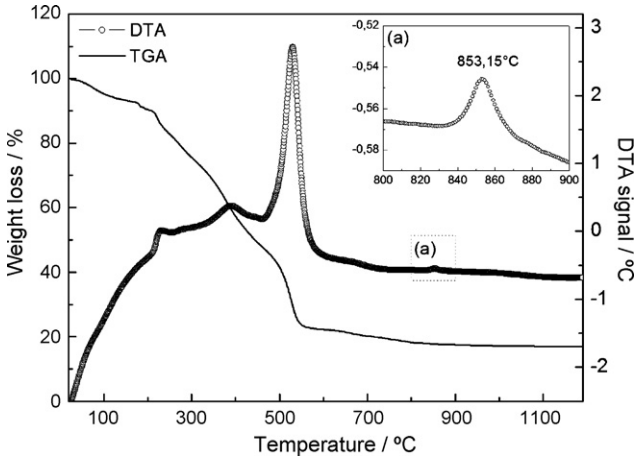

Fig. 2. TGA and DTA curves of the polymeric resin obtained by Pechini method.

3. Results and discussion

Fig. 2 presents the thermogravimetric analysis (TGA) and the differential thermal analysis (DTA) of the polymeric resin obtained by Pechini method. The TGA curve shows continuous weight loss, i.e., there is no formation of stable products during precursor decomposition, which is finished around 650 °C, as observed in DTA curve (exothermic peak at 530 °C). The exothermic peak approximately at 850 °C is due to the crystallization of $GdAlO_3$ phase. The crystallization temperature is low when compared to others methods, like sol–gel (900–1200 °C) and solid-state reactions (1450 °C) [7,12,13].

The X-ray diffraction patterns of $GdAlO_3:Eu^{3+}$ are shown in Fig. 3. According to XRD analysis (Fig. 3a), the fully crystalline single-phase $GdAlO_3$ could be obtained at 900 °C. The XRD patterns of samples obtained at 700 °C are characteristic of non-crystalline

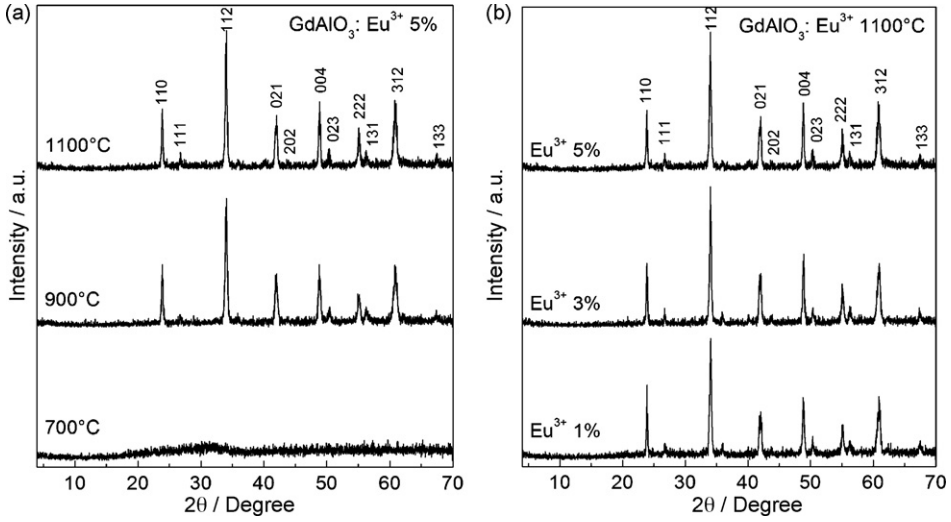

Fig. 3. X-ray diffraction patterns of $GdAlO_3:Eu^{3+}$ (a) temperature variation and (b) doping concentration variation.

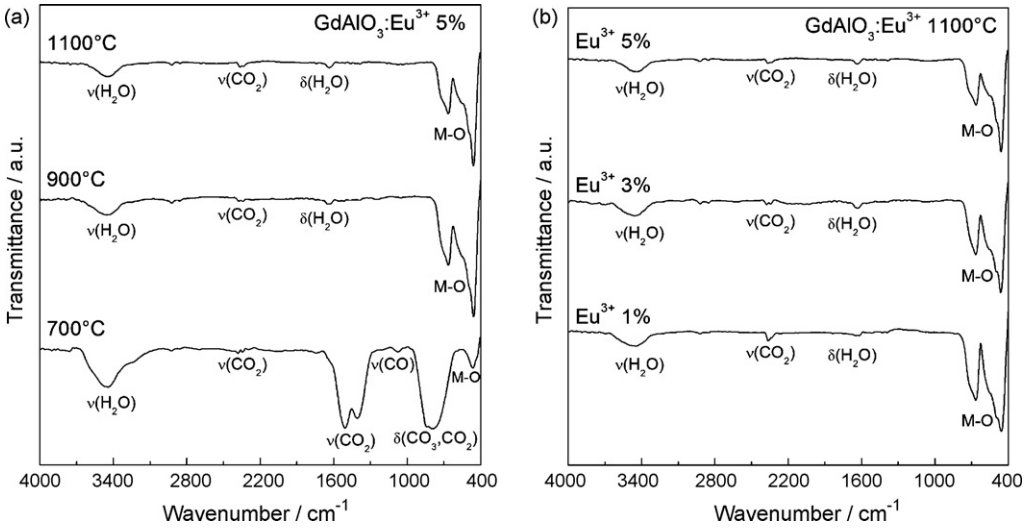

Fig. 4. FT-IR spectra of $GdAlO_3$:Eu^{3+} (a) temperature variation and (b) doping concentration variation.

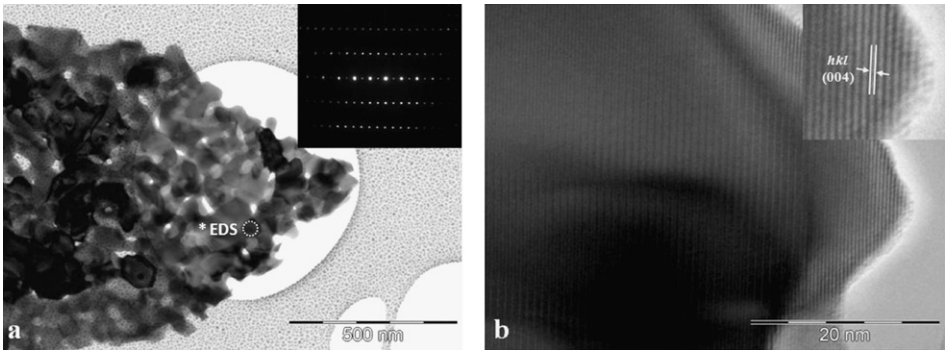

Fig. 5. (a) TEM image and (b) HRTEM image of $GdAlO_3$:Eu^{3+} 5 at%. *EDS spectrum is shown in Fig. 6.

solids. These results are consistent with crystallization temperature observed by TGA/DTA analysis. Fig. 3b shows that the doping concentration does not influence in the crystalline phase formation. All diffraction peaks in these XRD patterns could be attributed to the orthorhombic perovskite crystal structure of $GdAlO_3$ (JCPDF no. 46-395). The terbium-doped samples also exhibit the same behavior of the europium-doped samples in the XRD measurements.

The FT-IR spectra of $GdAlO_3$:Eu^{3+} samples obtained at different temperatures are shown in Fig. 4a. Only the sample obtained at 700 °C exhibits strong bands related to the residual organic matter probably originated from the incomplete decomposition of precursor polymeric resin at this temperature. Fig. 5b presents FT-IR spectra of the samples containing different doping concentrations obtained at 1100 °C. The spectral profiles are almost identical and exhibit strong bands between 400 cm^{-1} and 800 cm^{-1} which are typical metal–oxygen (Gd–O and Al–O) vibrations for the perovskite structure compounds. All spectra show a broadband around 3450 cm^{-1} and a narrow band at 1635 cm^{-1} assigned to the stretching and bending modes of adsorbed water, respectively. The spectra are representative of the Tb-doped samples. All characteristic absorption bands are summarized in Table 1.

The samples are composed by monocrystalline nanoparticles (mean diameter of 50–120 nm) and exhibit the formation of aggregates among them, showing a suitable ability for the sinterization (Fig. 5a). As can be seen in high resolution TEM images (Fig. 5b), the samples are highly crystalline. The TEM images showed in Fig. 5 are referent to $GdAlO_3$:Eu^{3+} 5% treated at 1100 °C. The lattice spacing corresponding to (0 0 4) and the distance is 1.86 Å. It is possible to observe peaks attributed at Al^{3+} and Gd^{3+} in the energy dispersive X-ray spectrum (EDS, Fig. 6). The peaks at 5.85 and 6.45 keV can be assigned to Eu^{3+} ions. Moreover, the absence of adjacent phases in XRD is evidence that Eu^{3+} is fully integrated into the $GdAlO_3$ host, forming solid solutions.

The excitation spectra of $GdAlO_3$:Eu^{3+} and $GdAlO_3$:Tb^{3+} samples were recorded fixing emission wavelength in 614 nm (Eu^{3+} $^5D_0 \rightarrow {}^7F_2$) and 542 nm ($Tb^{3+}$ $^5D_4 \rightarrow {}^7F_5$), respectively. The spectra are shown in Fig. 7. Excitation spectra of $GdAlO_3$:Eu^{3+} samples (Fig. 7a) present a broadband at 265 nm attributed to $O^{2-} \rightarrow Eu^{3+}$ charger transfer. The CT band energy of Eu^{3+} depends on the type of anion, the strength of binding of valence band electrons and on the size of the site occupied by Eu^{3+} ions. Following Dorenbos [14], in the rare earth aluminates, when the rare earth site occupied by the Eu^{3+} ions becomes smaller, the energy of the CT band tends to increase (shorter wavelength). Therefore, the energy of the Eu^{3+} CT band in $YAlO_3$ (ionic radius of Y^{3+} = 116 pm), $GdAlO_3$

Table 1
Characteristic absorption frequencies of the $GdAlO_3$:RE^{3+}.

Attribution	Frequency (cm^{-1})	Attribution	Frequency (cm^{-1})
δ Al–O (AlO_6)	455, 467, 495	υ_s (CO_2)	1384
Gd–O	555	υ_{ass} (CO_2)	1404, 1508
υ Al–O (AlO_6)	675	δ (H_2O)	1635
υ Al–O (AlO_4)	720, 772	υ_{ass} (CO_2)	2340
δ (CO_2)	788	υ_s (CH_2)	2364, 2856
δ_{ass} (CO_3)	840	υ_{ass} (CH_2)	2924
υ (CO)	1078	υ (OH)	3450

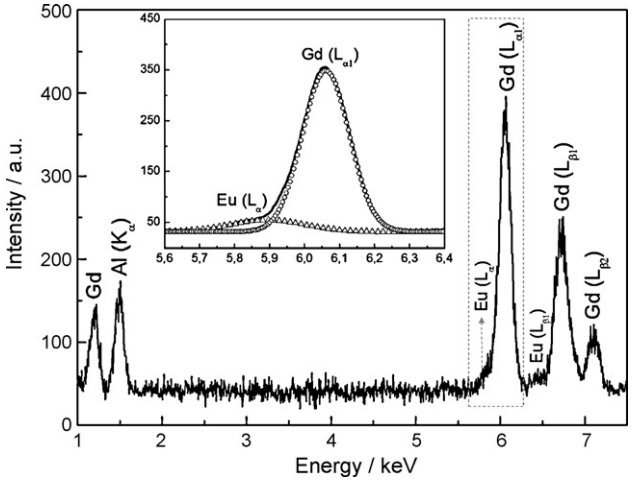

Fig. 6. EDS spectrum of $GdAlO_3$:Eu^{3+} 5 at%.

(Gd^{3+} = 119 pm), and $LaAlO_3$ (La^{3+} = 130 pm) are observed at 250 nm, 265 nm, and 314 nm, respectively. The results obtained in this work agree with Dorenbos [14] and Li et al. [15].

The sharp lines observed at the range 350–475 nm are assigned to *f*–*f* transitions of Eu^{3+} ions. The characteristics *f*–*f* transitions of Tb^{3+} ions are shown in Fig. 7b. The sharp lines observed in both spectra in 275 nm (Gd^{3+} $^8S_{7/2} \rightarrow {}^6I_{3/2}$), 312 nm and 318 nm ($Gd^{3+}$ $^8S_{7/2} \rightarrow {}^6P_j$) appear due to energy transfer from Gd^{3+} ions to RE^{3+} ions, $Gd^{3+} \rightarrow Eu^{3+}$, which occur from $^6I_{3/2}$ and ^6P_j Gd^{3+} level to the highest energy levels of RE^{3+} ions ($4f^7 5d$ or $4f^8$ configuration of Tb^{3+} and $4f^6$ configuration of Eu^{3+}) [16–18].

The emission spectra of Eu^{3+} and Tb^{3+}-doped samples obtained at different temperatures are shown in Fig. 8. The characteristics transitions of Eu^{3+} ions, $^5D_0 \rightarrow {}^7F_j$, are observed in all emission spectra (Fig. 8a). The $^5D_0 \rightarrow {}^7F_0$ transition around 579 nm suggests that the Eu^{3+} ions occupy at least one site without center of symmetry. Characteristics transitions of Tb^{3+} ions were also observed in all spectra. The assignments of blue and green emission of Tb^{3+} ions are showed in Fig. 8b.

Emission spectra of Eu^{3+} and Tb^{3+}-doped samples obtained at 700 °C present broad peaks, typical emission profile of non-crystalline compounds or highly disordered systems. The emission profile is similar when samples are excited at 275 nm or 399 nm (Eu^{3+}-samples) and 369 nm (Tb^{3+}-samples).

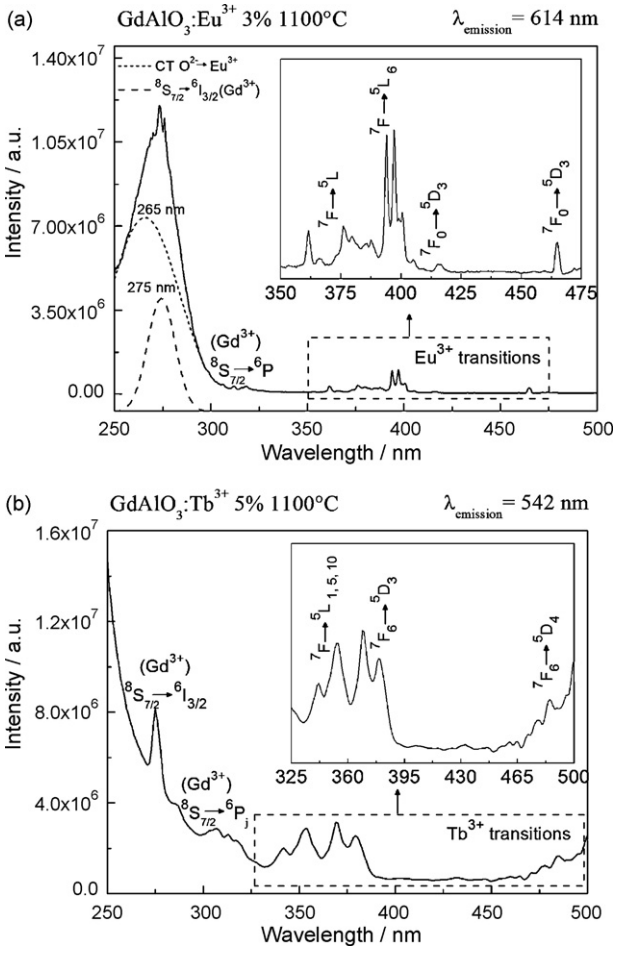

Fig. 7. Excitation spectra of (a) $GdAlO_3$:Eu^{3+} sample, $\lambda_{emission}$ = 614 nm and (b) $GdAlO_3$:Tb^{3+} sample, $\lambda_{emission}$ = 542 nm.

Fig. 9 presents the emission spectra of Eu^{3+} and Tb^{3+}-doped samples obtained at different doping concentrations. Fig. 9a shows that emission of $GdAlO_3$:Eu^{3+} at 1% presents low intensity and the sample containing Eu^{3+} at 3% exhibit the most intense emission. In the Eu^{3+}-samples at 5%, the luminescence is vanished because, in this concentration, the distance among dopant ions is short enough to

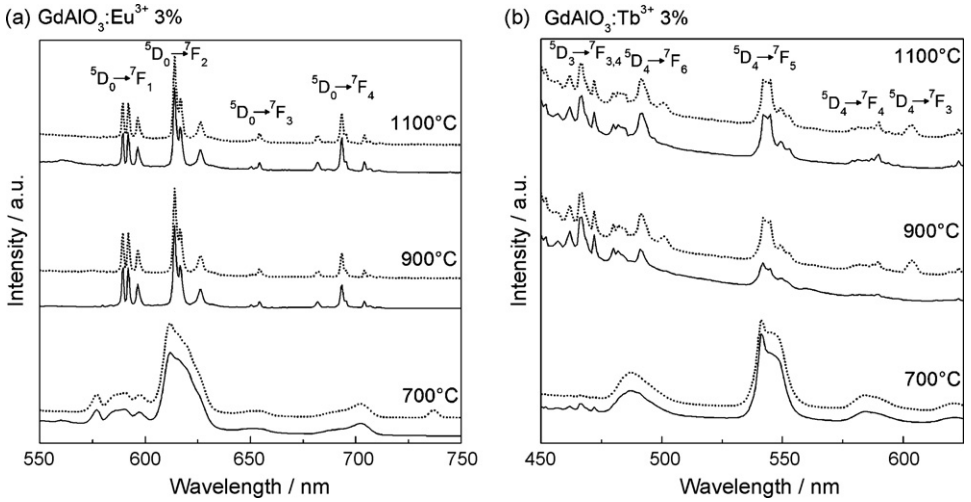

Fig. 8. (a) Emission spectra of $GdAlO_3$:Eu^{3+} samples. Excitation was fixed at 275 nm (continuous line) and 399 nm (dashed lines). (b) Emission spectra of $GdAlO_3$:Tb^{3+} samples. Excitation was fixed at 275 nm (continuous line) and 369 nm (dashed lines).

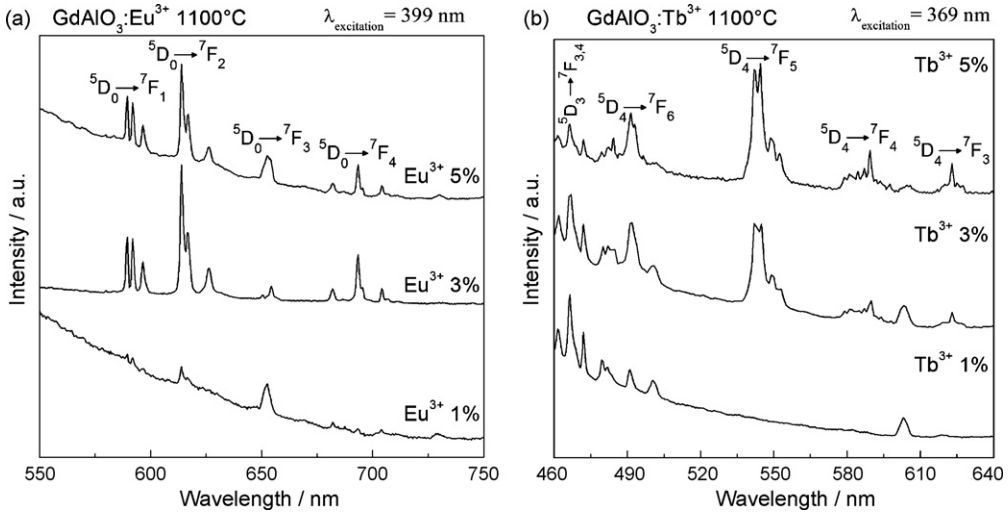

Fig. 9. Emission spectra of $GdAlO_3$:Eu^{3+} samples, $\lambda_{excitation}$ = 399 nm and (b) emission spectra of $GdAlO_3$:Tb^{3+} samples, $\lambda_{excitation}$ = 369 nm, obtained at different doping concentrations.

allow energy transfer, decreasing the emission intensity. The inclination observed in spectra of samples is due emission of Xe lamp utilized in spectrophotometer.

The emission spectra of $GdAlO_3$:Tb^{3+} are shown in Fig. 9b. At low Tb^{3+} concentrations, the blue emission from $^5D_3 \rightarrow {}^7F_j$ prevails. For higher Tb^{3+} concentrations, the blue emission decreases, followed by an increase in the green emission ($^5D_4 \rightarrow {}^7F_j$). This occurs because the well-known cross-relaxation process [18], where Tb^{3+} ion (donor) decay non-radioactively, $^5D_3 \rightarrow {}^5D_4$, and transfer energy to other Tb^{3+} ion (receptor). Thus, the emission occurs from $^5D_4$ (green emission). The process can be written as

$$Tb^{3+}(^5D_3) + Tb^{3+}(^7F_6) \rightarrow Tb^{3+}(^5D_4) + Tb^{3+}(^7F_0)$$

Therefore, the activator amount in the host determines the blue-green emission composition color. In the case of scintillators, more specifically for X-ray intensifying screens, the possibility of tuning $GdAlO_3$:Tb^{3+} emission defines the sensitivity of the photographic film used in the screen [18,19].

4. Conclusions

We reported the successful obtaining of $GdAlO_3$:RE^{3+} perovskites by the Pechini method at 700, 900 and 1100 °C. According to TGA/DTA analysis and XRD patterns, only samples fired at 900 and 1100 °C are crystalline. The FT-IR analysis showed that heat treatment at 700 °C is not sufficient for the complete precursor decomposition. TEM images show that particles are highly crystalline and present suitable ability for close-packing. The energy transfer $Gd^{3+} \rightarrow RE^{3+}$ was observed in excitation spectra. The RE^{3+} ions occupy at least one site without center of symmetry. The characteristic red emission of Eu^{3+} and the blue/green emission of Tb^{3+} was observed in photoluminescence measurements and the blue-green emission composition color of Tb^{3+}-samples can be tuned by amount doping.

Acknowledgements

The authors acknowledge support from the FAPESP, CNPq and RENAMI. H.H.S.O thanks FAPESP for scholarship.

References

[1] C. Greskovich, S. Duclos, Annual Review of Materials Science 27 (1997) 69.
[2] C.W.E. van Eijk, Nuclear Instruments and Methods in Physics Research A 392 (1997) 285.
[3] C.W.E. van Eijk, Nuclear Instruments and Methods in Physics Research A 460 (2001) 1.
[4] M.J. Weber, Journal of Luminescence 100 (2002) 35.
[5] G. Blasse, Journal of Alloys and Compounds 225 (1995) 529.
[6] S.E. Derenzo, et al., Nuclear Instruments and Methods in Physics Research A 505 (2003) 111.
[7] S. Cizauskaite, et al., Materials Chemistry and Physics 102 (2007) 105.
[8] C.R. Stanek, et al., Journal of Applied Physics 99 (2006) 113518.
[9] S.A. Smirnova, et al., Journal of Luminescence 60 and 61 (1994) 960.
[10] G. Hai, et al., Applied Surface Science 243 (2005) 245.
[11] United State Patent Office, M.P. Pechini. US 3330697 (11th July 1967).
[12] J.W.M. Verweij, et al., Chemical Physics Letters 239 (1995) 51.
[13] S. Chaudhury, et al., Journal of Solid State Chemistry 180 (2007) 2393.
[14] P. Dorenbos, Journal of Luminescence 111 (2005) 89–104.
[15] Y. Wang, et al., Journal of Solid State Chemistry 177 (2004) 2242–2248.
[16] Y.C. Li, et al., Materials Science and Engineering B 146 (2008) 225.
[17] H. Gao, Y. Wang, Journal of Luminescence 122 and 123 (2007) 997.
[18] A.A. da Silva, et al., Journal of Luminescence 128 (2008) 1165.
[19] L.H. Brixner, Materials Chemistry and Physics 16 (1987) 253.